

Young protoplanetary disks

Tom Douglas^{1*}, Paola Caselli¹, Et al.

¹School of Physics and Astronomy, University of Leeds, Leeds LS2 9JT, UK

In original form 2012

ABSTRACT

Abstract here

Key words: circumstellar matter – infrared: stars.

1 INTRODUCTION

The formation and early evolution of protoplanetary disks around solar-type and low-mass protostars has little observational support, despite of the fast growing list of theoretical models on the dynamical evolution of star forming dense cores (e.g. Krasnopolsky et al. 2011; Machida et al. 2011; Braiding & Wardle 2012). The reason for this is that young protostars are surrounded by thick envelopes and power energetic outflows, thus observations of the young disks, predicted to have sizes of about 100 AU and masses as large as 10% the original core mass (e.g. Joos et al. 2012), are challenging. The use of sensitive interferometers is needed to achieve high angular resolution and spatially/spectrally disentangle the various (disk + envelope + outflow) components as well to filter out the extended emission tracing envelope material.

After the pioneer work of, e.g., Chandler et al. (1995), Brown et al. (2000), Looney et al. (2000), recent interferometric observations have discovered compact embedded disks in a sample of Class 0 (André et al. 2000) sources, finding masses between 0.4 and $>1 M_{\odot}$ (Jørgensen et al. 2007, 2009; Enoch et al. 2011). A 130 AU disk was discovered toward a Class 0 source in Perseus, using Jansky Very Large Array (JVLA) observations of NH₃ (Choi et al. 2007). Pineda et al. (2012) observed methyl formate with the Atacama Millimeter and sub-millimeter Array (ALMA) and found evidence of rotation toward one of the protobinary Class 0 sources embedded in IRAS 16293-2422. These observations are consistent with an almost edge-on disk. When ALMA will be completed, it will be finally possible to spatially resolve these young disks and, for the first time, put stringent constraints on theoretical models. As full-operational ALMA is fast approaching, it is important to provide observational predictions based on dynamical models of young protoplanetary disks.

In this paper, we focus our attention to the young self-gravitating disks of Boley & Durisen (2008), where episodic heating induced by spiral shocks is present, as this may be a good representation of the earliest phases of protoplan-

etary disks and an alternative to the young "static" disks studied by, e.g. Visser et al. (2009, 2011). As shown by Ilee et al. (2011), the spiral shocks cause desorption of volatiles from dust icy mantles and trigger gas-phase chemical reactions with activation energies, which are inactive at lower temperatures. These processes produce clear chemical signatures of the disk dynamics. With the use of 3D radiative transfer modeling, we perform simulated ALMA observations of the disk studied by Ilee et al. (2011) and identify the best tracers of the physical structure of self-gravitating disks. The physical, chemical and radiative transfer models are described in Sect 2. Radiative transfer results are in Sect. 3, while ALMA simulated observations are in Sec. 4. Discussions and conclusions can be found in Sect. 5.

2 DESCRIPTION OF THE MODEL

2.1 Physical and chemical structure

The physical model used to simulate the emission from a young protoplanetary disc is a hybrid model obtained from embedding a gravitationally unstable protoplanetary disk within an envelope with characteristics similar to the well-studied pre-stellar core L1544, as derived by Keto & Caselli (2010; hereafter KC2010). The KC2010 model follows the dynamical, chemical and thermal evolution of a contracting Bonnor-Ebert (Bonnor 1956; Ebert 1957) sphere with total mass of $10 M_{\odot}$, until it reaches the density, temperature and velocity profiles which best match observations. The pre-stellar core model adopted here contains slight modifications due to the inclusion of oxygen cooling in the outer regions of the cloud, where CO is mostly photodissociated (Keto et al., in preparation), and it is shown in Fig. 2.1.

The pre-stellar core structure is maintained down to a radius of 80 AU, within which the young protoplanetary disk has been plugged in. The disk structure is derived by the hydrodynamic model of Boley(2007) and Boley (2009). The particular model considered here (as well as in Ilee et al. 2011) is a $0.39 M_{\odot}$ self-gravitating disc featuring prominent spiral arms. H₂ number densities in the disc range from $10^{10}\text{--}10^{19} m^{-3}$, and temperatures range from

* E-mail: pytd@leeds.ac.uk

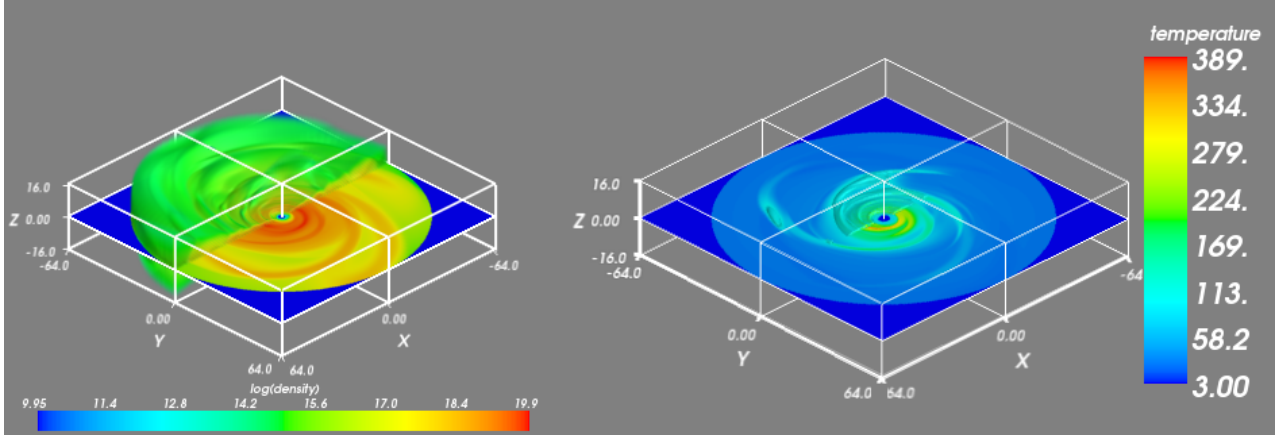


Figure 1. Left: A 3D plot of log number density (m^{-3}) showing the spiral structure in the xy plane and scale height of the disc. Right: The 3D temperature structure of the disc; regions cooler than 40 degrees are not shown in 3D, demonstrating the narrow central region containing hot material.

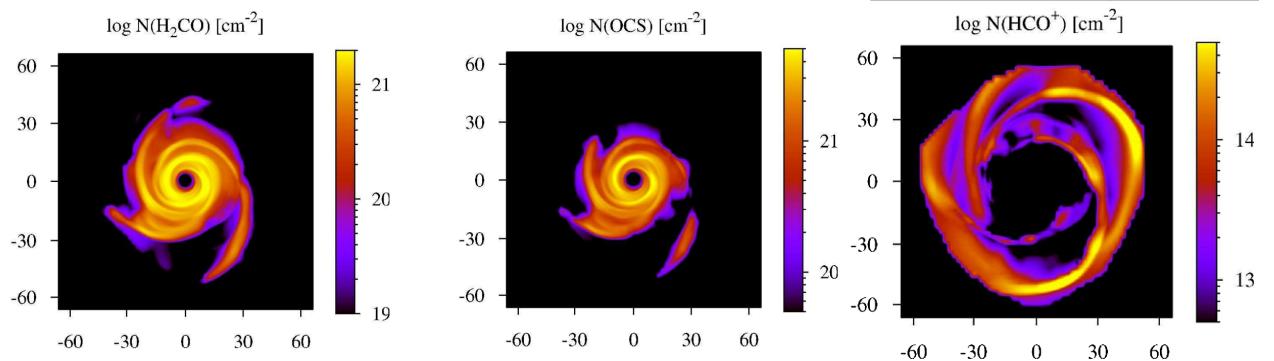


Figure 2. Column densities of H_2CO , OCS and HCO^+ used in the disc model. Figure adapted from Ilee et al. (2011)

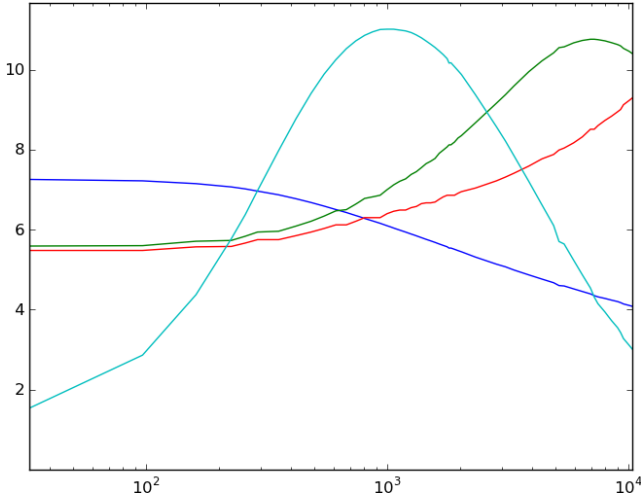


Figure 3. Model of the pre-stellar core L1544 used as the envelope of the young protoplanetary disk in the hybrid model. Showing temperature (red) and dust (green) temperature in kelvin, log number density (blue) in cm^{-3} and inward velocity $\times 100$ (cyan) in m s^{-1} . Adapted from Keto & Caselli (2010) and Keto et al. (2012, in preparation).

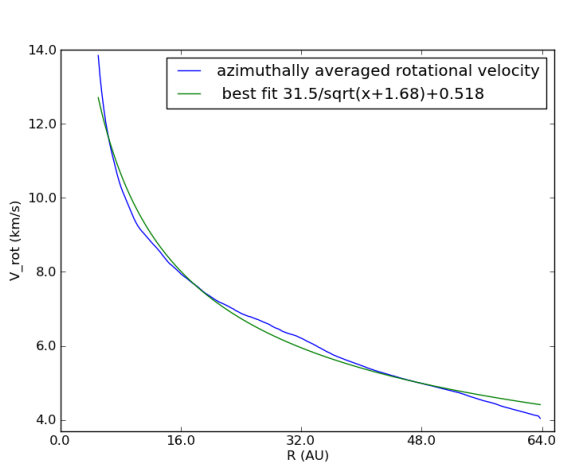


Figure 4. Azimuthally averaged rotational velocity in the disc mid-plane with best fit curve

30–400 K (figure 2.1). The dust and gas temperatures in the disc are assumed to be in equilibrium. The model is sampled over a regular grid of size $256 \times 256 \times 64$ with spatial resolution of 0.5 au in x , y and z . The gas/dust

mass ratio was assumed to be 1/100 throughout both sections model and the opacities were given by the model of dust grains with thick icy mantles and 10^6 yr coagulation from Ossenkopf and Henning (1994). The gas number density and temperature structure are displayed in Fig. XX.

Chemical abundances in the disc were taken from Ilee et al (2011) which followed the changes of chemical abundances of trace particles moving through the disc as it evolved. The abundances of 125 species related by 1334 reactions were followed through the time evolution of the disc. These abundances were interpolated onto a 51^3 grid covering the disc with cells of size $2.2 \times 2.2 \times 0.22$ au. Fig. XX shows a sample of column density maps from Ilee et al. (2011), pointing out the different regions traced by H₂CO and OCS, which mostly probe the central warm regions, and HCO⁺, which preferentially trace the outer spiral pattern as in the central region is destroyed by water molecules (see Ilee et al. 2011 for details). The simple chemistry in the KC2010 model, adopted here as the envelope of the protoplanetary disk, does not provide detailed abundances of molecular species (besides CO and H₂O, see also Caselli et al. 2012). As discussed in the result section (Sec. 3), rough guesses have been made based on values measured toward similar object.

2.2 The radiative transfer code

The radiative transfer program used, LIME (Brinch & Hogerheijde 2010), calculates line intensities based on a weighted sample of randomly chosen points in a continuous 3D model. The method of selecting these points is given in the gridding section. At each of these points, the density of the main collision partner (H₂), gas and dust temperatures, velocity, molecular abundances and turbulent velocity are taken from the model. These points are then smoothed by Lloyds algorithm (Lloyd 1982) in order to minimise the variation in distance between points whilst keeping the same underlying distribution. These points are then connected by Delaunay triangulation¹ and it is down these paths that photon propagation is restricted (figures 2.2). The level populations of the selected molecules are calculated at each of these points from collisional and radiative (de)excitation and the local radiation field is calculated. This is repeated 20 times with the populations of each level converging towards a single value. This number of iterations is sufficient for the signal to noise ratio of the level populations (as defined in Brinch & Hogerheijde 2010) to exceed 1000 in 99% of the points

2.3 Grid Construction

In order to construct the grid, points are randomly selected from the volume then have the density and molecular density at the point compared against a reference point in

¹ In three dimensions this means that if four points are connected into a tetrahedron, the sphere circumscribing these four points contains no other points. It can be shown that this connection is unique for a given set of points.

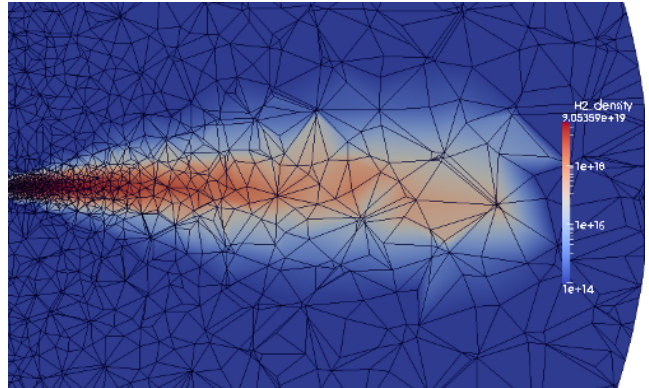


Figure 5. A plot of the points selected by the gridding process and the paths down which photons can propagate overlaid on a smoothed density model. The points are more concentrated at small radii and in the densest regions.

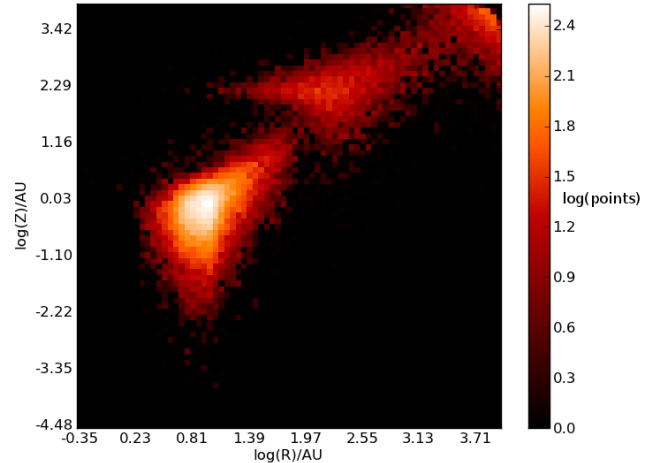


Figure 6. A histogram of the point distribution throughout the model. The disc and envelope can be seen as two separate entities which have to be sampled using different point distributions

order to decide if the point is to be accepted or not. Grid points are selected at random in cylindrical co-ordinates, linearly spaced in z and ϕ and logarithmically spaced in r . For each point to be selected, a random number α is drawn from the semi-open set $[0, 1)$ as a threshold. After selection of random co-ordinates, the hydrogen density and molecular density at the point (n and m , respectively) are compared against the densities of a reference point on the inner edge of the disc (n_0 and m_0). If $\alpha < (\frac{n}{n_0})^{0.3}$ or $\alpha < (\frac{m}{m_0})^{0.3}$ then the point is selected for use, if not then another r , ϕ , z co-ordinate is selected. The weighting function and point distribution were selected empirically to sample all the scales while ensuring that the majority of points are located in the inner disc where the density is higher. 20% of these points are forced to be at radii greater than $\sqrt{R_{min}R_{max}}$ (where R_{min} and R_{max} are the inner and outer radius of the model) in order to stop too many of the selected points clustering in the high density disc and leaving the envelope undersampled. In addition to this method of

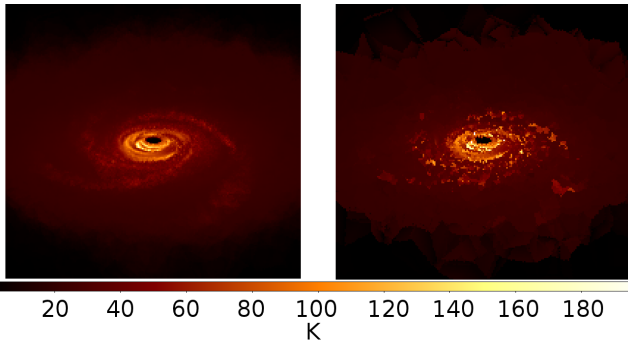


Figure 7. A plot showing the difference between a single LIME continuum image at 300 GHz (right) and the average of ten such images from different runs of the same model in LIME (left).

selection, 5% of the points are linearly distributed in x , y and z with no bias with regards to density or abundance. This provides a minimum level of sampling for the large low density regions in the outer parts of the simulated volume. See figure 2.2 for an example of the points distribution in r , z .

3 MODEL RESULTS

Simulated molecules were confined to species where the chemical abundance in the disc and envelope are known, or have simulated abundances. In addition radiative transfer simulations are limited to are limited to molecules where the collisional and Einstein co-efficients are known. Lines for these molecules were simulated with LIME for frequencies 50~500 GHz, with focus on lines which could be observed in ALMA band 7. The results presented in this section represent those lines which show detectable emission/absorption which can be used to trace either spiral structure or rotation.

The results of these simulations for the molecules OCS, HCO^+ , H_2CO and isotopologues of CO are shown here, other molecules simulated but not shown include HCN, HNC, HNO, HCS $^+$ and CS. For the purpose of simulating observations the model was placed at roughly the distance of nearby low-mass star forming regions (100 pc) and is inclined at 30° to edge on. From these observations integrated intensity, intensity weighted velocity and position velocity diagrams through the centre of the model were created. The simulations done are focused upon frequencies within ALMA band 7, selected to give the best trade off between resolution and sensitivity for early ALMA science **IS BAND 7 STILL THE BEST FOR US TO LOOK AT SEEING AS WE ARE NOW LOOKING AT ALMA FULL CAPABILITY RATHER THAN CYCLE1?** (Note the moment 1 and 0 maps were created by integrating between -12.5 to -0.5 km s^{-1} and +0.5 to +12.5 km s^{-1} to avoid being dominated by the contribution from the envelope, this can be seen in some PV diagrams as the strong absorption feature at all positions around zero velocity, moment 1 maps are shown with a cutoff of 1/1000 of the peak emission/absorption value)

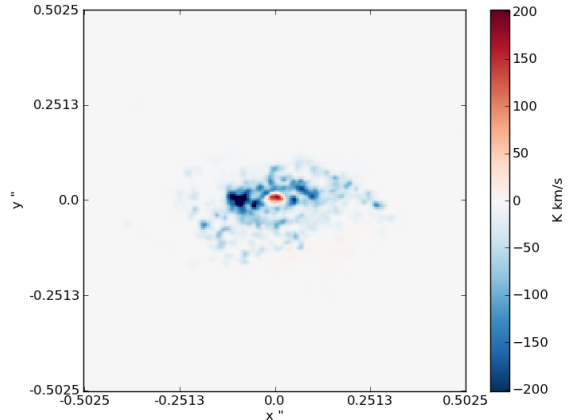


Figure 8. CO J=3-2 Continuum subtracted mom0

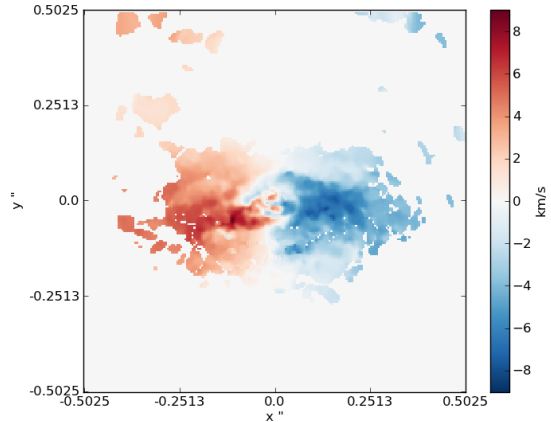


Figure 9. CO J=3-2 moment 1 map

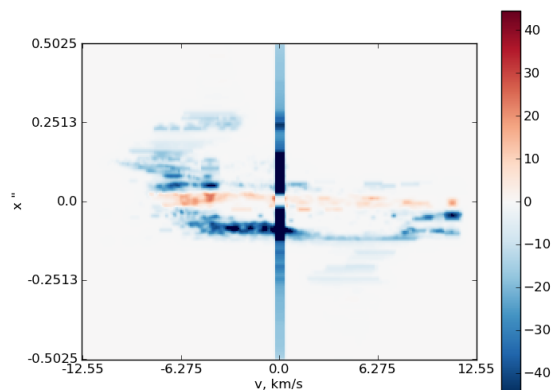


Figure 10. CO J=3-2 PV through $y=0$

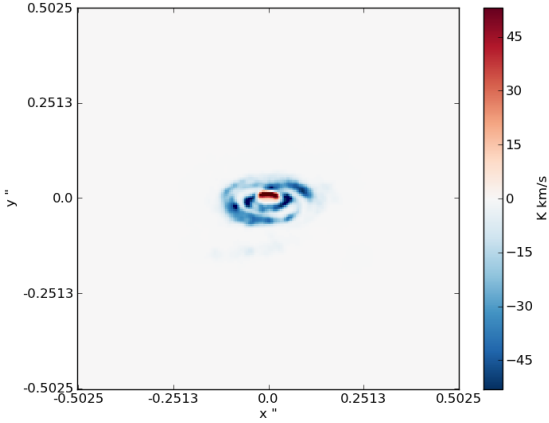


Figure 11. OCS 28-27 Continuum subtracted mom0

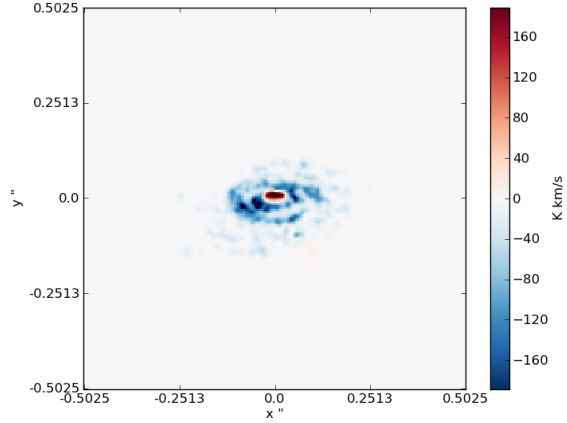


Figure 13. H₂CO 404 - 303 Continuum subtracted mom0

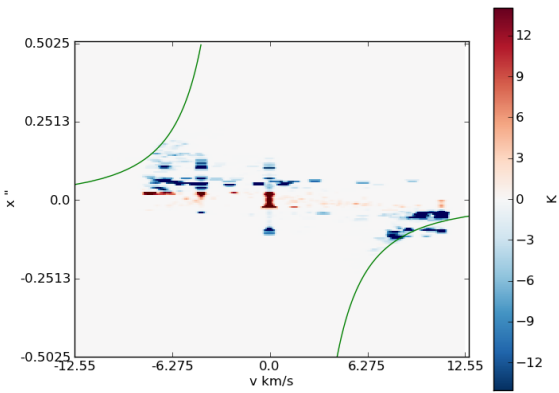


Figure 12. OCS 28-27 PV through centre

Figures 6,7 and 8 show synthetic images of the CO J=3-2 line at 345.8 GHz. As the upper level for this line is at 33 K above the ground state this transition should be excited throughout the disc. Given the large and uniform nature of the abundance of CO in the disc this line will be optically thick and this is only mapping the outer regions of the disc. In common with most transitions simulated, the line is seen almost exclusively in absorption against the disc continuum. The region of emission in the centre is where there is no continuum background to be absorbed. Some indications of spiral structure can be seen but are indistinct. **not sure how useful these are, might be worth cutting them?**

After looking at a variety of lines which could be observed of ALMA band 6 or 7 (211-275 GHz and 275-373 GHz) we found that the OCS lines in ALMA band 7 (22-21 through 30-29) with upper energy levels between 161 and 271 K above the ground state provide a way to trace hot shocked gas in spiral arms without resolving structure. Figures 3 & ?? show the integrated intensity of the OCS J=28-27 line in the model described previously and one

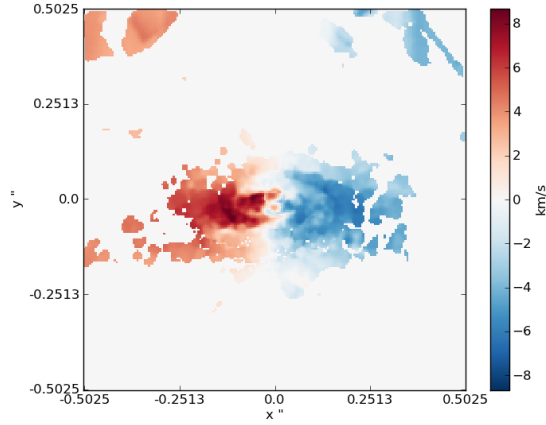


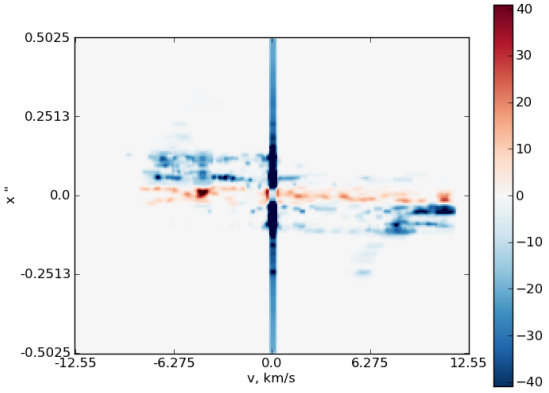
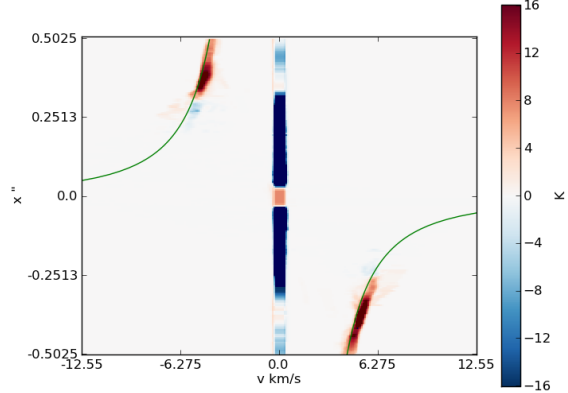
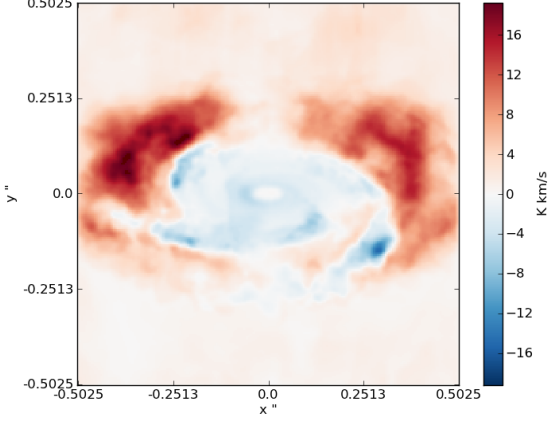
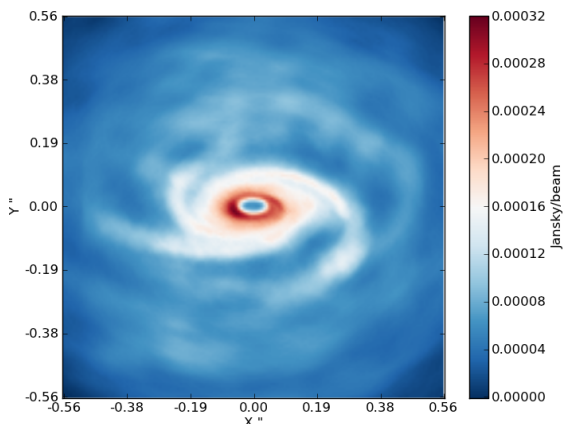
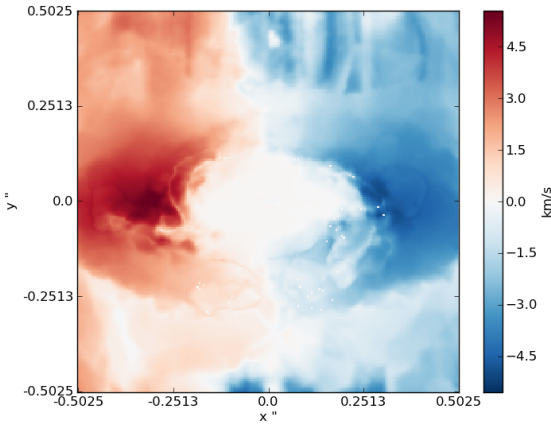
Figure 14. H₂CO 404 - 303 PV through centre

where the disc section of the model is an axis-symmetric model created by taking the azimuthal average of density, temperature and molecular abundance. The order of magnitude difference in the line intensity provides a method to detect hot dense gas without being able to resolve the spiral structure spatially.

More complex molecules such as H₂CO with many closely spaced spectral lines can be used to gain an estimate on the temperature of a region.

Some molecules such as HCO⁺ trace only the outer regions of the disc (Ilee 2011) and so can be used to look at the extended velocity and physical structure. In these colder less dense regions we see the molecular lines in emission rather than absorption. Figure ?? shows the rotation curve of the model as shown in figure 2.1 against the HCO⁺ J=1-0 line emission. It is clear that from observations such as these the rotation curve of a disc could be reconstructed.

In all the simulations except HCO⁺ we see molecular lines in absorption throughout the majority of the disc and

**Figure 15.** H₂CO 404 - 303 PV through centre**Figure 18.** HCO⁺ 1-0 pv through centre, with the rotation curve from figure 2.1 for comparison**Figure 16.** HCO⁺ 1-0 Continuum subtracted mom0**Figure 19.** continuum emission at 337GHz simulated for ALMA most extended configuration**Figure 17.** HCO⁺ 1-0 mom1map

in some cases a small amount of emission towards the centre. Molecular lines throughout the plane of the disc show up in absorption against the continuum emission of the shock heated, dense midplane.

4 ALMA PREDICTIONS

5 DISCUSSION AND CONCLUSIONS

In this paper we have performed radiative transfer simulations of a hybrid model comprising a $0.4 M_{\odot}$ self gravitating disc with radius $64 AU$ showing spiral density waves, surrounded by an envelope simulated as a collapsing $10 M_{\odot}$ BE-sphere. CASA simulations show that at a distance of $100 pc$ both spatial resolution of the spirals in such a disc and extraction of kinematic and temperature from molecular lines are possible in ALMA band 7. Our simulations show that many molecular species are predominantly seen in absorption towards the centre of self-gravitating protoplanetary discs. The quiescent nature of the envelope around such discs only obscures them within $\pm 0.5 km s^{-1}$.

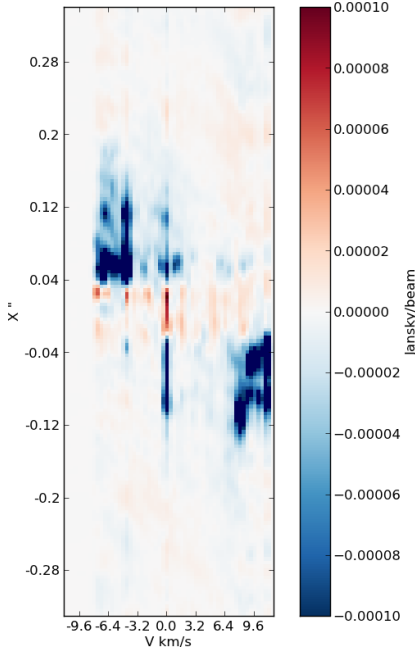


Figure 20. OCS 28-29 pv diagram simulated for ALMA most extended configuration

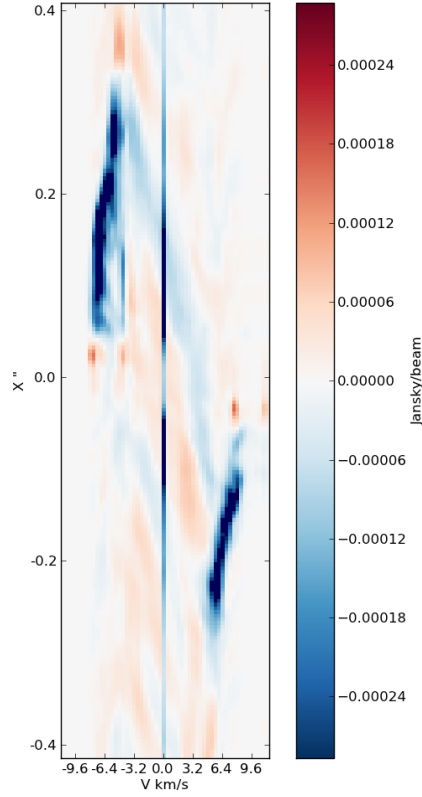


Figure 22. C17O 3-2 30 deg PV through centre simulated for ALMA most extended configuration

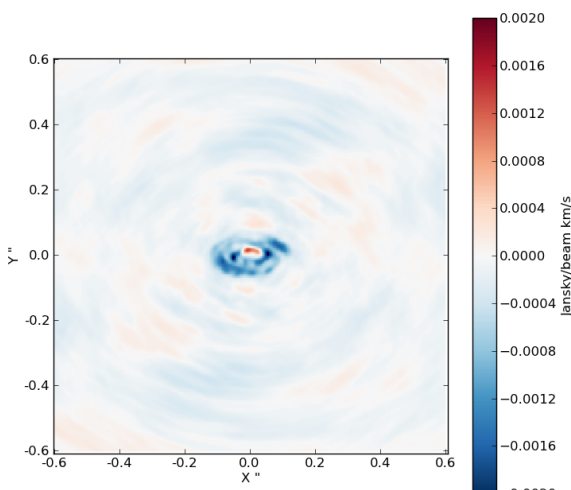


Figure 21. OCS 28-29 integrated intensity simulated for ALMA most extended configuration

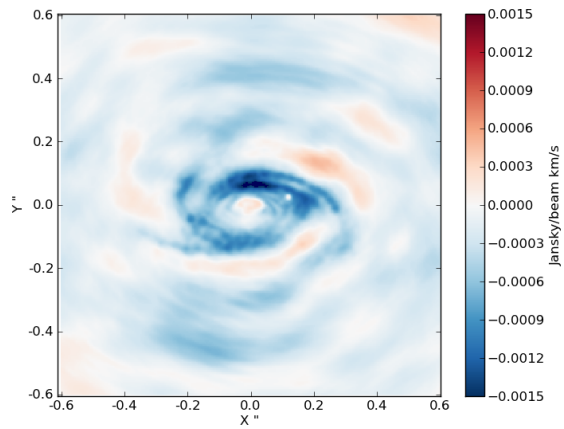


Figure 23. C17O 3-2 30 deg integrated intensity simulated for ALMA most extended configuration

One assumption made in this model is that the gas and dust are in thermal equilibrium. If they are not and the dust is significantly cooler than the gas then transitions may not show up in absorption.

In the model spirals shock heat the mid-plane layer and the colder more diffuse gas absorbs the continuum from it, this results in molecular lines being seen in absorption whenever lines of sight pass through the cold diffuse gas at larger heights on to the hot dense midplane of the disc. Rotation curves can be gathered from these observations even with spiral structure

Outflows could contaminate measurements of rotation curves meaning that species which commonly trace outflows, such as CO and HCO⁺ are not going to be good tracers of disc rotation. However species such as OCS and C¹⁸O which are not commonly seen in outflows (Yildiz et al 2012,) can be used to trace disc rotation.

ACKNOWLEDGEMENTS

stuff here

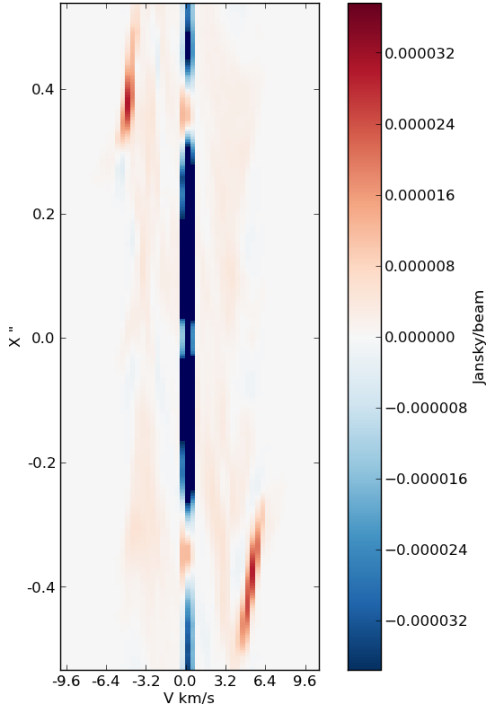


Figure 24. HCO^+ 1-0 30 deg PV through centre simulated for ALMA most extended configuration

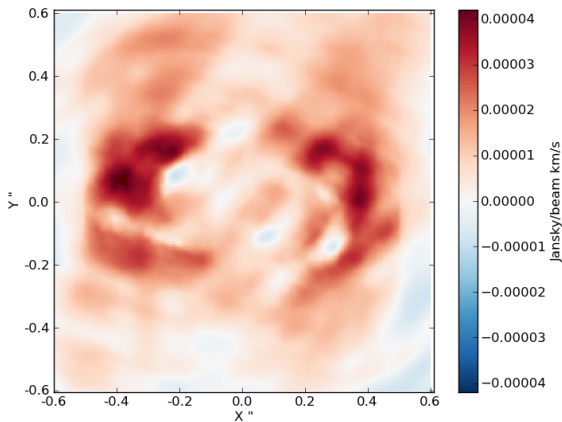


Figure 25. HCO^+ 1-0 30 deg integrated intensity simulated for ALMA most extended configuration

APPENDIX A: OTHER INCLINATIONS

Figures showing different inclinations

This paper has been typeset from a \TeX / \LaTeX file prepared by the author.

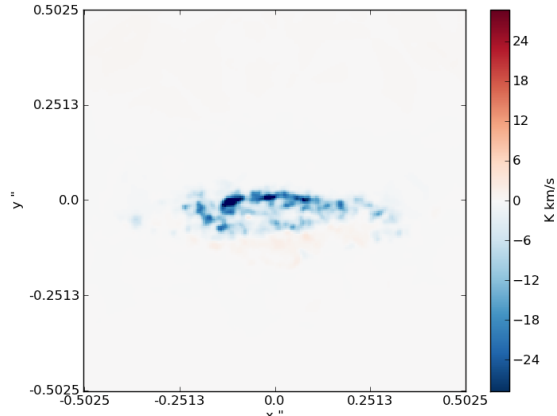


Figure A1. C18O 3-2 15 deg Continuum subtracted mom0

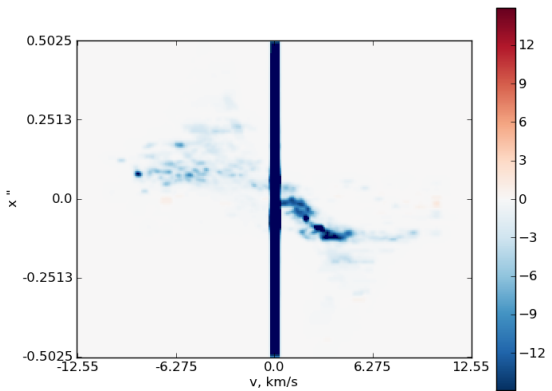


Figure A2. C18O 3-2 PV 15 deg through centre

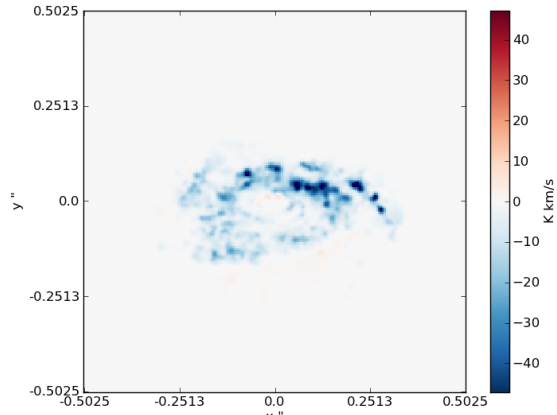


Figure A3. C18O 3-2 30 deg Continuum subtracted mom0

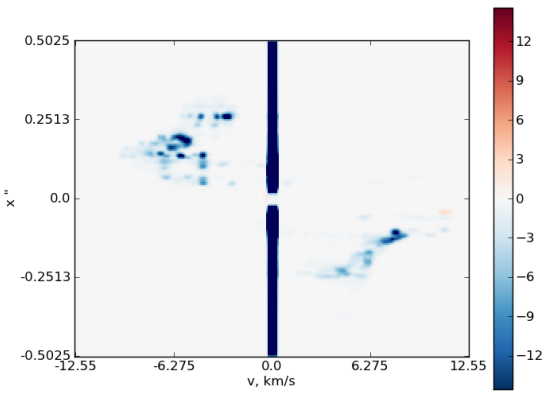


Figure A4. C18O 3-2 30 deg PV through centre

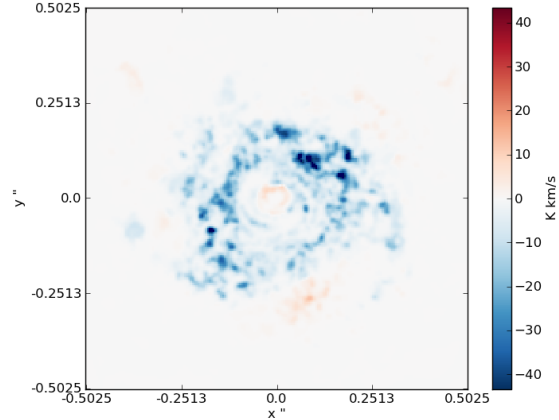


Figure A7. C18O 3-2 60 deg Continuum subtracted mom0

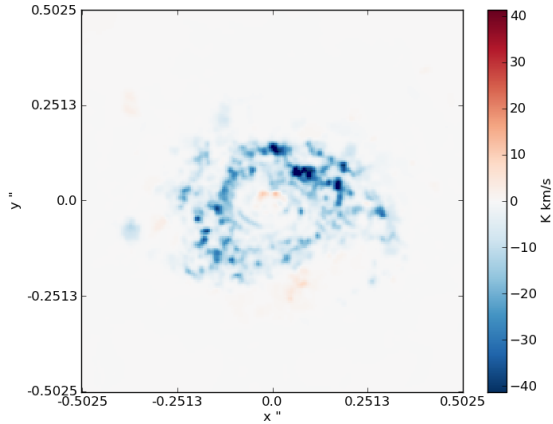


Figure A5. C18O 3-2 45 deg Continuum subtracted mom0

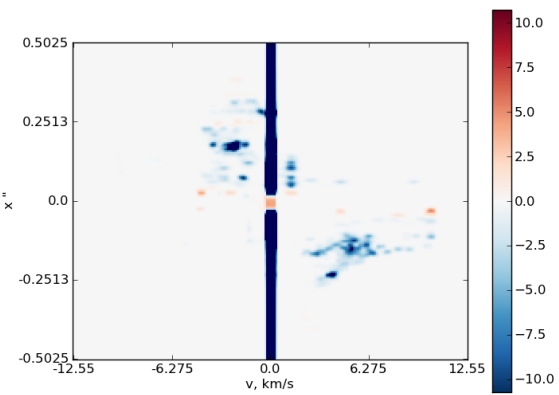


Figure A8. C18O 3-2 60 deg PV through centre

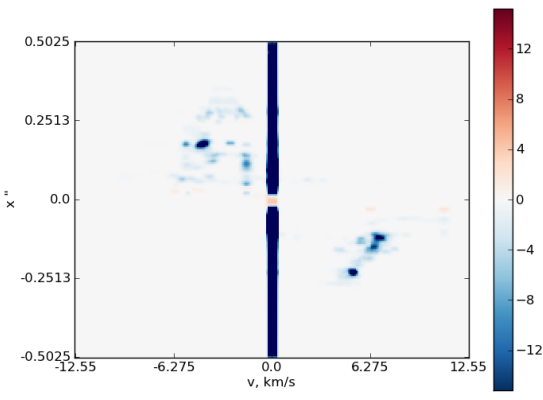


Figure A6. C18O 3-2 45 deg PV through centre

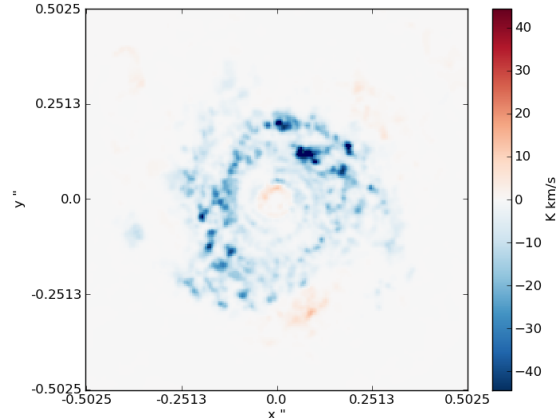


Figure A9. C18O 3-2 75 deg Continuum subtracted mom0

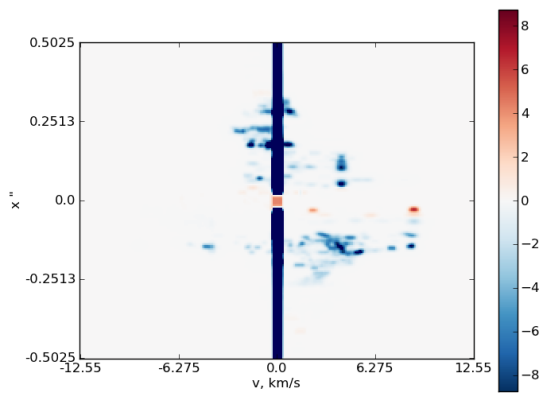


Figure A10. C₁₈O 3-2 75 deg PV through centre